Nano Energy (2014) **7**, 134–142

Available online at www.sciencedirect.com

ScienceDirect

journal homepage: www.elsevier.com/locate/nanoenergy

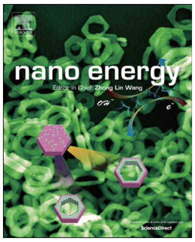

RAPID COMMUNICATION

Co_3O_4@layered double hydroxide core/shell hierarchical nanowire arrays for enhanced supercapacitance performance

Fanyu Ning, Mingfei Shao, Chenglong Zhang, Simin Xu,
Min Wei*, Xue Duan

State Key Laboratory of Chemical Resource Engineering, Beijing University of Chemical Technology, Beijing 100029, PR China

Received 30 March 2014; received in revised form 26 April 2014; accepted 2 May 2014
Available online 10 May 2014

KEYWORDS
Layered double hydroxides;
Core/shell nanowire arrays;
Hierarchical architecture;
Supercapacitors

Abstract
Co_3O_4@NiAl-layered double hydroxide (LDH) core/shell nanowire arrays with hierarchical structure have been synthesized by *in situ* growth of LDH nanosheets shell on the surface of Co_3O_4 nanowire arrays. The resulting Co_3O_4@NiAl-LDH material exhibits promising supercapacitance performance with largely enhanced specific capacitance and rate capability, much superior to pristine Co_3O_4 nanowire arrays. The improvement in electrochemical behavior is attributed to the hierarchically mesoporous morphology and the strong core-shell binding interaction, which facilitates a sufficient exposure of electroactive species as well as the charge transportation process. This work provides a facile and effective strategy for the fabrication of hierarchical materials with core/shell structure, which can be potentially used in the energy storage and conversion devices.

Introduction

One-dimensional (1-D) nanowire arrays with excellent charge transportation property have attracted considerable interest for their potential applications in optoelectronics [1,2], electronics [3,4], sensors [5] and electrochemical energy storage devices [6–10]. However, the deficient exposure of surface active site [11–13] and slow interfacial reaction kinetics [14] largely limit their applications as electrode materials in electrochemical devices. Great efforts have been devoted to enhance the electrochemical performance of nanowire arrays. The fabrication of hierarchical shell on 1-D nanowire arrays can be a promising

---

*Corresponding author. Tel.: +86 10 64412131; fax: +86 10 64425358.
E-mail address: weimin@mail.buct.edu.cn (M. Wei).

http://dx.doi.org/10.1016/j.nanoen.2014.05.002
2211-2855/© 2014 Elsevier Ltd. All rights reserved.

solution because this core/shell architecture combines the large specific surface area of hierarchical shell [15-17] and the reliable electric connection between active species and the current collector provided by the nanowire core [18,19]. Moreover, with suitable micro-/nanostructural design, hierarchical core/shell nanowire arrays can make use of both components and show a potential synergistic effect [20-22]. Various materials including metals [23], metal oxides/hydroxides [24,25], carbonaceous materials [26,27] and polymers [28] have been integrated into this kind of core/shell structures by different methods (*e.g.*, hydrothermal synthesis [20], oxidation [29], chemical bath deposition [21], electrodeposition [24], sputtering [30] and pulsed laser deposition [31]). Despite all these progresses, the rational design and facile fabrication of core/shell hierarchical nanowire arrays with well-defined morphology and enhanced property still remain a big challenge.

Layered double hydroxides (LDHs) are well-known hydrotalcite-like anionic clays with general formula $[M^{II}_{1-x}M^{III}_{x}(OH)_2]^{x+}[A^{n-}]_{x/n}\cdot mH_2O$ (M^{II} and M^{III} are divalent and trivalent metals respectively, and A^{n-} is interlayer anion). Due to their versatility in matrix composition and interlayer anions [32,33], LDH materials have been widely used in catalysis [34,35], visible-light photocatalysis [36], optical materials [37], magnetics [38], biology [39] and electrochemical devices [40]. Recently, LDHs have been reported as electrode materials in supercapacitors because of their desirable properties including low cost, high redox activity and environmental friendliness nature [41,42]. However, low electrical conductivity and aggregation of active species greatly restrict their charge transportation and result in unsatisfactory supercapacitance performance [43]. Therefore, it is highly essential to construct a sophisticated architecture that enables sufficient exposure of electroactive species as well as fast ion/electron transfer for LDHs to achieve excellent supercapacitance behavior. Various materials such as LDH/carbon composite [44-46], three-dimension LDH microsphere [47] and LDH nanoplatelet arrays [27,43,48] have been reported and show desirable performance. However, hierarchical LDHs shell coated 1-D nanowire arrays for supercapacitive applications has not been reported.

Co_3O_4 is one of the most promising pseudocapacitive materials due to its low toxic, low cost and extremely high theoretical specific capacitance (3560 F g^{-1}), but commonly suffers from low practical specific capacitance (90 − 754 F g^{-1}) and poor rate capability [6,49,50]. Herein, we present the design and fabrication of Co_3O_4@LDH core/shell hierarchical nanowire arrays by *in situ* growth of LDH nanosheets shell on the surface of Co_3O_4 nanowires core. This material shows the following merits: (i) the Co_3O_4 nanowires core on conductive substrate provides a direct electrical pathway from active species to the current collector; (ii) the hierarchical architecture of LDH shell enables effective exposure of active center for Faradaic redox reaction and thus enhances the interfacial charge transmission; (iii) the reasonable combination of two kinds of pseudocapacitance-active species (Co_3O_4 and LDH) can probably achieve a potential synergistic effect. The as-obtained Co_3O_4@NiAl-LDH core/shell nanowire arrays exhibit largely enhanced specific capacitance (1772 F g^{-1} at 2 A g^{-1}), good rate capability (61.4% retention at 20 A g^{-1}) as well as cycling performance (87.9% capacitance was retained after 2000 cycles at 8 A g^{-1}). Therefore, this work provides a facile approach for the fabrication of core/shell hierarchical nanowire arrays materials, which can be potentially used in supercapacitors.

Experimental section

Synthesis of Co_3O_4@LDH hierarchical nanowire arrays

All of the reactants in the experiments were of analytical grade and used without any further purification. The fabrication process of Co_3O_4@LDH core/shell hierarchical nanowire arrays is shown in Figure 1.

Preparation of Co_3O_4 nanowire arrays

The Co_3O_4 nanowire arrays were prepared by a facile hydrothermal synthesis method according to previous report [51]. Typically, 5 mmol of $Co(NO_3)_2\cdot 6H_2O$, 10 mmol of NH_4F, and 25 mmol of $CO(NH_2)_2$ were dissolved in 50 ml of deionized water under stirring, and then was transferred into a Teflon-lined stainless steel autoclave. A piece of clean nickel foam (2 cm × 5 cm in size) substrate was immersed into the above solution, with the top side coated with a polytetrafluoroethylene tape to prevent the solution contamination. The autoclave was sealed and maintained at 120 °C for 5 h. After the reaction, the substrate was washed thoroughly with deionized water, followed by calcination at 350 °C in air for 2 h.

Preparation of Co_3O_4@AlOOH nanowire arrays

The AlOOH primer sol was firstly prepared according to our previous work [49]. Co_3O_4@AlOOH nanowire arrays were then prepared *via* a sol-gel process. The obtained Co_3O_4 nanowire substrate was immersed in the AlOOH primer sol for the self-assembly of AlOOH sol onto the surface of Co_3O_4 nanowires. After 30 min, the substrate was transferred into ethanol for 10 min and rinsed with ethanol several times to remove unanchored AlOOH sol. Finally, the substrate was dried at 60 °C in air for 2 h.

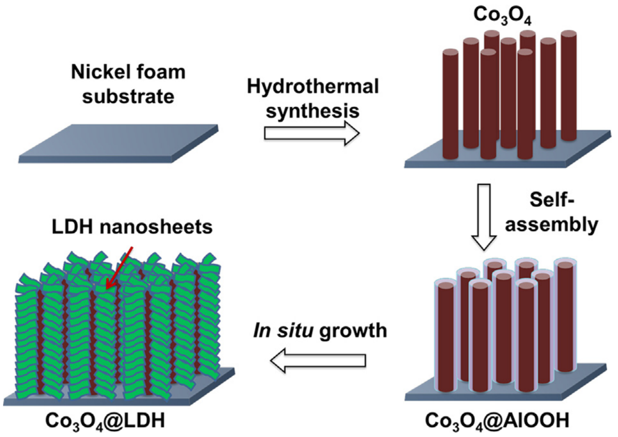

Figure 1 Schematic illustration for the fabrication of Co_3O_4@LDH core/shell hierarchical nanowire arrays on nickel foam substrate.

Preparation of Co_3O_4@LDH core/shell nanowire arrays

The *in situ* growth of hierarchical LDH nanosheets shell on the surface of Co_3O_4 nanowire arrays was carried out. For Co_3O_4@NiAl-LDH, 0.7 mmol of $Ni(NO_3)_2 \cdot 6H_2O$ and 16 mmol of $CO(NH_2)_2$ were dissolved in 70 ml of deionized water. The homogeneous solution was transferred into a Teflon-lined stainless steel autoclave. Subsequently, the Co_3O_4@AlOOH nanowire arrays substrate was placed in the reaction solution, sealed and maintained at 100 °C for 24 h. After cooling to room temperature, the resulting Co_3O_4@NiAl-LDH core/shell nanowire arrays substrate was collected and rinsed with deionized water. The preparation of Co_3O_4@MgAl-LDH and Co_3O_4@ZnAl-LDH nanowire arrays was performed with a similar method by using $Mg(NO_3)_2 \cdot 6H_2O$ and $Zn(NO_3)_2 \cdot 6H_2O$, respectively.

Material characterization

X-ray diffraction (XRD) patterns were collected on a Rigaku XRD-6000 diffractometer using Cu Kα radiation. The morphology was investigated using a scanning electron microscope (SEM; Zeiss SUPRA 55) with an accelerating voltage of 20 kV, combined with energy dispersive X-ray spectroscopy (EDS). Transmission electron microscope (TEM) images were recorded using a JEOL JEM-2010 h-TEM with an accelerating voltage of 200 kV. A Tecnai G2 F30 S-TWIN microscope operated at 300 kV was employed to reveal the core-shell structure using the scanning transmission electron microscope (STEM) mode with EDS mapping. Elemental analysis for metal element was performed using a Shimadzu ICPS-75000 inductively coupled plasma-atomic emission spectrometer (ICP-AES). Fourier transform infrared spectra (FT-IR) were recorded on a Bruker Vector-22 Fourier transform spectrometer. X-ray photoelectron spectroscopy (XPS) measurements were performed on a Thermo VG Escalab 250 X-ray photoelectron spectrometer with Al Kα radiation at a pressure of $\sim 2 \times 10^{-9}$ Pa.

Electrochemical characterization

Electrochemical measurements were performed on an electrochemical workstation (CHI 660C, CH Instruments Inc., Shanghai) using a three-electrode mood in 6 M KOH aqueous solution. The Co_3O_4@NiAl-LDH core/shell nanowire arrays and pristine Co_3O_4 nanowire arrays (1.0 cm × 1.0 cm; $m_{Co_3O_4} \approx 2.7$ mg cm^{-2}; $m_{\text{NiAl-LDH}} \approx 1.2$ mg cm^{-2}) on Ni foam substrate were directly used as the working electrode. The reference electrode and counter electrode were saturated calomel electrode (SCE) and platinum electrode, respectively. Cyclic voltammetry (CV) was performed in a potential range from -0.2 V to 0.5 V at 0.05 V s^{-1}. Galvanostatic (GV) charge/discharge measurements were carried out within the potential window from -0.1 V to 0.4 V at various specific currents. Electrochemical impedance spectroscopy (EIS) tests were performed by applying an AC voltage with 5 mV amplitude in a frequency range from 100 kHz to 0.1 Hz. The specific capacitance was calculated according to the following equation: $C = It/\Delta Vm$, where C is the specific capacitance; I is the constant discharge current; t is the discharge time; ΔV is the potential drop during discharge, and m is the mass of total active species (both Co_3O_4 and NiAl-LDH). The specific energy was calculated by the following equation: $E = C\Delta V^2/2$, where E is the specific energy; C is the specific capacitance, and ΔV is the potential drop during discharge. The specific capacitance per surface area was calculated by the following equation: $C_{SA} = It/\Delta VS$, where C_{SA} is the specific capacitance per surface area; I is the constant discharge current; t is the discharge time; ΔV is the potential drop during discharge, and S is the surface area of electrode.

Results and discussion

Firstly, the Co_3O_4 nanowire arrays grown on nickel foam were synthesized *via* a facile hydrothermal method according to previous work [51]. As shown in Figure 2A, the Co_3O_4 nanowires were uniformly and densely oriented vertical to the substrate with an average diameter of ~160 nm and a length of ~8 μm (Figure S1). After coating a thin layer of AlOOH *via* a sol-gel process, no obvious change in morphology can be observed (Figure 2B). Finally, the Co_3O_4@LDH core/shell nanowire arrays were obtained *via* a hydrothermal method in an alkaline solution containing metal ions. Typically, the AlOOH layer deposited on the surface of Co_3O_4 nanowires acts as the interfacial reactive template for the growth of LDH nanosheets shell. Figure 2C displays typical images of Co_3O_4@NiAl-LDH core/shell nanowire arrays. Co_3O_4 nanowires are coated with uniform LDH nanosheets (~180 nm in lateral size and ~12 nm in thickness), which interconnect with each other and form a highly porous surface morphology. The as-obtained core/shell nanowire arrays (~550 nm in diameter) maintain a uniform orientation vertical to the substrate. EDS mapping analysis (Figure 2D) shows that cobalt is located in the central part of the core/shell nanowire while nickel is distributed homogeneously in the whole nanowire; EDS spectrum (Figure S1) also displays the presence of Co, Ni, and Al with Co/Ni/Al molar ratio of 15:5:1. In addition, both Co_3O_4@MgAl-LDH and Co_3O_4@ZnAl-LDH nanowire arrays (Figure S2) show similar core-shell structure and branched morphology with LDH nanosheets perpendicularly grafted to the Co_3O_4 nanowires core. The Co/M(II)/Al molar ratios of these Co_3O_4@M(II)Al-LDH (M=Ni, Mg, Zn) samples were obtained by ICP-AES and the results are listed in Table S1. The Co/Ni/Al molar ratio in Co_3O_4@NiAl-LDH core/shell nanowire arrays is 11.89:4.30:1, which approximately agrees with the EDS spectrum. Moreover, the FT-IR spectra (Figure S3) demonstrate the existence of interlayer NO_3^- anions for the synthesized NiAl-LDH, MgAl-LDH and ZnAl-LDH.

Figure 3 shows the XRD patterns of nickel foam substrate, Co_3O_4 nanowire arrays, Co_3O_4@AlOOH nanowire arrays and Co_3O_4@LDH core/shell nanowire arrays. The diffraction peaks in curve b (except those of nickel substrate) with dominant (311) reflection can be indexed to the cubic spinel Co_3O_4 (JCPDS card no. 42-1467). After coating with a AlOOH layer, no obvious change can be observed (Figure 3, curve c), indicating an amorphous phase of AlOOH layer. The reflections of both LDHs and Co_3O_4 are observed in the case of Co_3O_4@NiAl-LDH core/shell nanowire arrays (Figure 3, curve d). The (003), (006) and (012) reflections indicate a typical LDH phase with high crystallinity [47]. In addition, Figure S4 displays the XRD patterns of powdered samples of

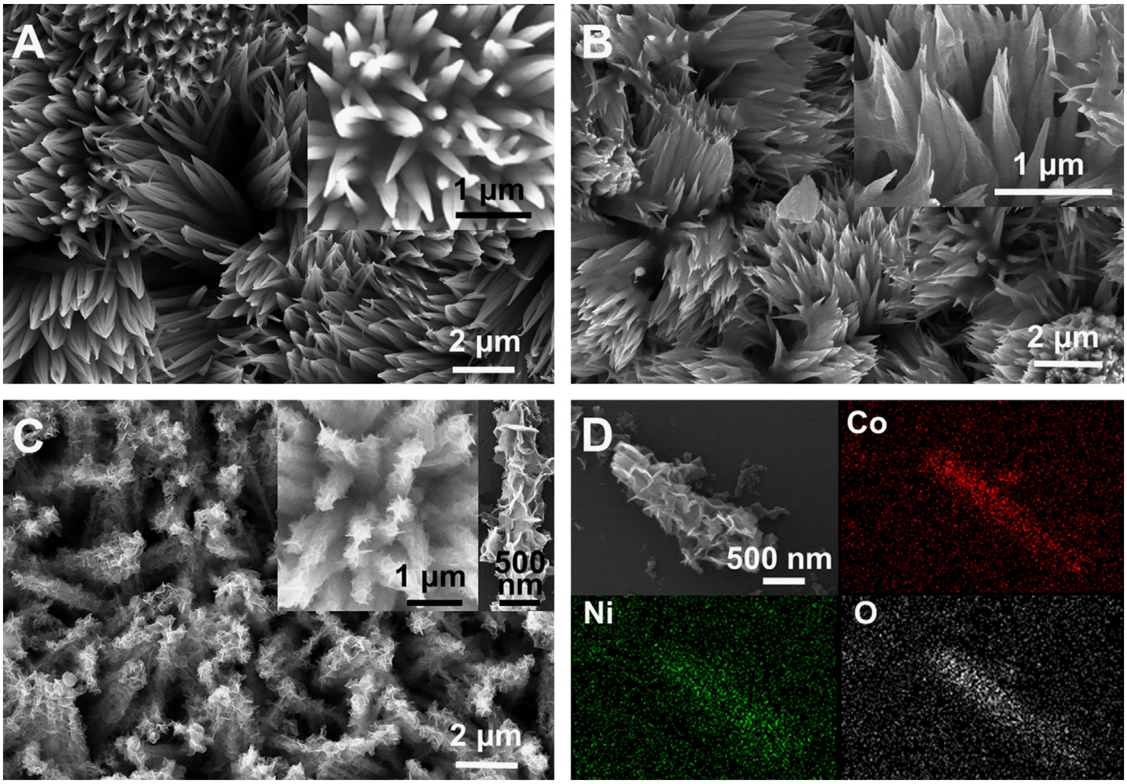

Figure 2 SEM images of (A) Co_3O_4 nanowire arrays, (B) Co_3O_4@AlOOH nanowire arrays, (C) Co_3O_4@NiAl-LDH core/shell nanowire arrays (the inset shows enlarged image). (D) EDS mapping in SEM for a single Co_3O_4@NiAl-LDH nanowire.

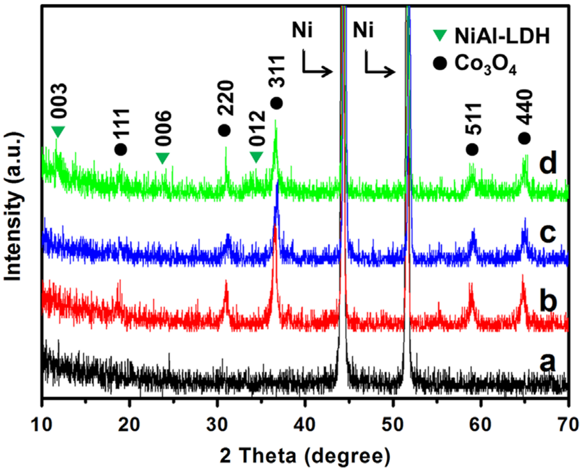

Figure 3 XRD patterns of: (a) nickel foam substrate, (b) Co_3O_4 nanowire arrays on nickel foam, (c) Co_3O_4@AlOOH nanowire arrays on nickel foam, (d) Co_3O_4@NiAl-LDH core/shell nanowire arrays on nickel foam.

Co_3O_4, Co_3O_4@AlOOH and Co_3O_4@LDH scratched from the substrate, which exhibit a high accordance with those of nanowire arrays on the substrate (Figure 3).

Figure 4A shows a typical TEM image of an individual Co_3O_4@NiAl-LDH core/shell nanowire, in which the Co_3O_4 nanowire core and NiAl-LDH nanosheets shell can be easily distinguished. The Co_3O_4 nanowire core is composed of nanocrystallites (10–20 nm in size), and the NiAl-LDH nanosheets are anchored to the surface of Co_3O_4 nanowire core. The detail nanostructure is further investigated by HRTEM. As shown in Figure 4B, the NiAl-LDH nanosheets are densely connected to Co_3O_4 core without any evident amorphous interface. Lattice fringes corresponding to interplanar distance of 0.47 nm and 0.28 nm can be indexed to the (111) and (220) plane of spinel Co_3O_4 phase, and interplanar distance of 0.25 nm can be attributed to the (012) plane of NiAl-LDH phase. Moreover, the distortion of lattice fringes for both Co_3O_4 and NiAl-LDH in the interface region demonstrates a strong interaction between the core and shell [53]. In addition, the core-shell structure of Co_3O_4@NiAl-LDH nanowires was further identified by the EDS mapping analysis of Co, Ni and Al in STEM (Figure 4C-F), in which Co is located in the core region while Ni and Al are distributed homogeneously in the whole nanowires shell.

The interaction between Co_3O_4 core and LDH shell was further investigated by X-ray photoelectron spectroscopy (XPS) measurements. Figure 5 shows the typical Co 2p, Ni 2p, O 1s, and Al 2p XPS spectrum of Co_3O_4, Co_3O_4@AlOOH and Co_3O_4@NiAl-LDH sample. The peaks were decomposed by mixed Gaussian–Lorentzian fitting and Shirley background was used to substrate the background. For the sample of Co_3O_4 nanowire arrays (Figure 5A, curve a), The Co $2p_{3/2}$ peak can be decomposed to two peaks located at 779.2 and 780.6 eV, accompanied with decomposed Co $2p_{1/2}$ peaks located at 794.5 and 795.9 eV, indicating the existence of both Co (II) and Co (III) oxidation state in the surface, respectively [54]. After the coating of AlOOH layer, both $Co2p_{3/2}$ and Co $2p_{1/2}$ peak shift to lower energy region with sharply decreased intensity (Figure 5A, curve b), and the Co $2p_{3/2}$ peak only presents at 779.2 eV while the peak at 780.6 eV disappeared. Such an observation indicates that

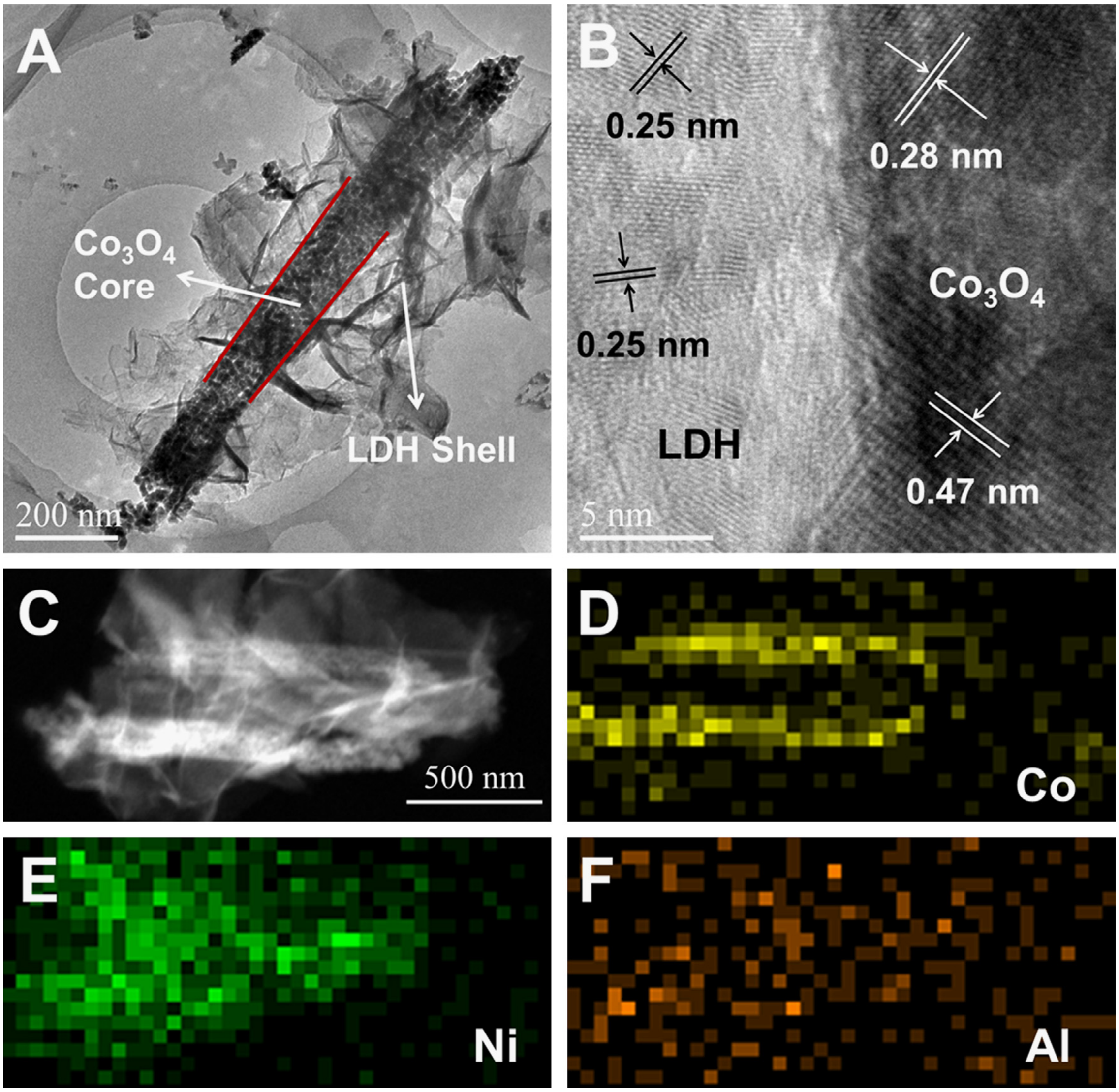

Figure 4 (A) TEM image and (B) HRTEM image of an individual Co_3O_4@NiAl-LDH core/shell nanowire. (C) STEM image and (D—F) corresponding EDS mapping results.

the surface Co species exists as Co(III) oxidation state. This valence change possibly results from the oxidization of surface Co^{2+} in Co_3O_4 nanowires by HNO_3 in the AlOOH primer sol during the coating process. For the sample of Co_3O_4@NiAl-LDH core/shell nanowire arrays (Figure 5A, curve c), the Co $2p_{3/2}$ peak shifts to higher energy level and is mainly composed of the peak at 780.6 eV, indicating the Co (II) oxidation state corresponding to the Co atoms in $Co(OH)_2$ [55]. The formation of $Co(OH)_2$ is related to the binding of Co on the surface of Co_3O_4 core and OH group of NiAl-LDH shell, implying a strong chemical bond between Co_3O_4 core and LDH shell. This interaction may enable effective charge transportation at the core-shell interface [56]. The Ni 2p core lines of Co_3O_4@NiAl-LDH nanowire arrays sample (Figure 5B, curve a) split to Ni $2p_{3/2}$ (855.4 eV) and Ni $2p_{1/2}$ (873.1 eV) peak accompanied with two satellite bands at 861.2 and 878.9 eV, which implies the presence of a high-spin Ni^{2+} in NiAl-LDH [57,58]. In addition, the O 1s core level spectrum (Figure 5C) was deconvoluted to three peaks located at 529.6, 531 and 532.8 eV, corresponding to O atom in metal oxide (Co_3O_4), hydroxyl group (AlOOH and NiAl-LDH), and absorbed water, respectively. From Co_3O_4 (Figure 5C, curve c) to Co_3O_4@AlOOH (Figure 5C, curve b) and then to Co_3O_4@NiAl-LDH (Figure 5C curve a), the peak at 531 eV increases while the one at 529.6 eV decreases gradually, further confirming the deposition of AlOOH and the subsequent *in situ* growth of NiAl-LDH on the surface of Co_3O_4 nanowire arrays. Figure 5D shows that the Al 2p peak is located at 74.4 eV, which indicates the Al(III) oxidation state of Al element in NiAl-LDH.

The electrochemical property of hierarchical Co_3O_4@NiAl-LDH core/shell nanowire arrays grown on nickel foam for supercapacitor was investigated. Figure 6A shows the cyclic voltammograms (CVs) of the nickel foam substrate, Co_3O_4 nanowire arrays and Co_3O_4@NiAl-LDH core/shell nanowire arrays in 6 M KOH at a scan rate of 0.05 V s^{-1}. No evident redox peak was observed for the nickel foam substrate (black curve in Figure 6A), indicating that the capacitance of the substrate is negligible. For the Co_3O_4 nanowire arrays, two pairs of redox peaks at ~0.25 and 0.35 V are

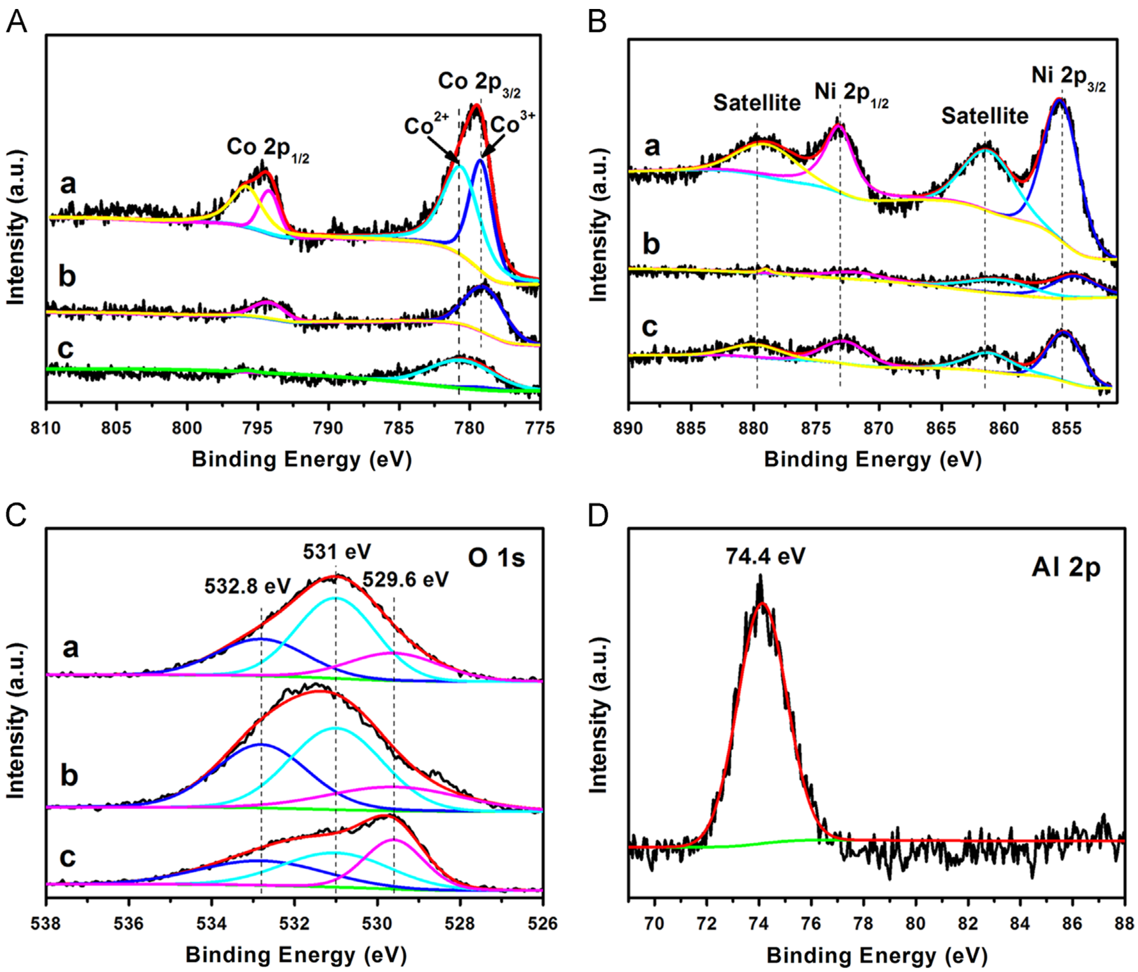

Figure 5 (A) typical Co 2p XPS spectra of: (a) Co_3O_4, (b) Co_3O_4@AlOOH, (c) Co_3O_4@NiAl-LDH. (B) Ni 2p XPS spectra of: (a) Co_3O_4@NiAl-LDH, (b) Co_3O_4@AlOOH, (c) Co_3O_4. (C) O 1s XPS spectra of: (a) Co_3O_4@NiAl-LDH, (b) Co_3O_4@AlOOH, (c) Co_3O_4. (D) Al 2p XPS spectrum of Co_3O_4@NiAl-LDH core/shell nanowire arrays.

observed, corresponding to Co^{2+}/Co^{3+} and Co^{3+}/Co^{4+} associated with OH^-, respectively (red curve in Figure 6A) [20,21]. In the case of Co_3O_4@NiAl-LDH core/shell nanowire arrays (green curve in Figure 6A), only the redox peaks belonging to Ni^{2+}/Ni^{3+} in the NiAl-LDH associated with OH^- are observed [59]. The redox peaks of Co_3O_4 core are probably superimposed by those of NiAl-LDH shell because of the rather high redox current density of Ni^{2+}/Ni^{3+}. Obviously, the peak current of Co_3O_4@NiAl-LDH increases dramatically in comparison with that of pristine Co_3O_4, indicating the largely enhanced electrochemical reaction activity of core/shell nanowire arrays.

Galvanostatic charge/discharge measurements were further performed on pristine Co_3O_4 and Co_3O_4@NiAl-LDH nanowire arrays. Since the pristine Co_3O_4 nanowire arrays cannot be charged to 0.5 V due to the oxidation evolution reaction (as shown in Figure S5), a relatively small potential window range from −0.1 to 0.4 V was chosen, so as to give a better comparison study between the two kinds of electrode materials. The charge/discharge characteristics of both nanowire arrays are consistent with the results of CVs, which exhibit a typical pseudocapacitive behavior. The corresponding specific capacitance is 1772 and 444 $F\,g^{-1}$ for Co_3O_4@NiAl-LDH core/shell nanowire arrays and Co_3O_4 nanowire arrays, respectively, at a current density of 2 $A\,g^{-1}$. The Co_3O_4@NiAl-LDH core/shell nanowire arrays shows a great enhancement in pseudocapacitive performance, superior to the Co_3O_4 sample and some previously reported Co_3O_4-based materials, such as Co_3O_4 nanosheet@-nanowire arrays [52], Co_3O_4@MnO_2 core/shell nanowire arrays [20], and Co_3O_4@NiO core/shell nanowire arrays [21] (Table S2).

The rate capability of Co_3O_4@NiAl-LDH and Co_3O_4 nanowire arrays were investigated by galvanostatic charge/discharge measurements at various charge/discharge current densities. The resulting charge/discharge curves are shown in Figure S6 and the derived specific capacitances are displayed in Figure 6C. For Co_3O_4@NiAl-LDH core/shell nanowire arrays electrode, the specific capacitance at a high current density of 20 $A\,g^{-1}$ (1088 $F\,g^{-1}$) maintains 61.4% of the specific capacitance at 2 $A\,g^{-1}$ (1772 $F\,g^{-1}$), whereas the pristine Co_3O_4 nanowire arrays one only keeps at 48.4% (from 444 $F\,g^{-1}$ to 216 $F\,g^{-1}$). In addition, Figure S7 shows the capacitance per surface area, from which the Co_3O_4@NiAl-LDH still exhibits much higher capacitance (6.9 $F\,cm^{-2}$ at 7.8 $mA\,cm^{-2}$) than that of Co_3O_4 (1.2 $F\,cm^{-2}$ at 5.4 $mA\,cm^{-2}$). The enhancement in specific capacitance and rate capability of Co_3O_4@NiAl-LDH sample mainly

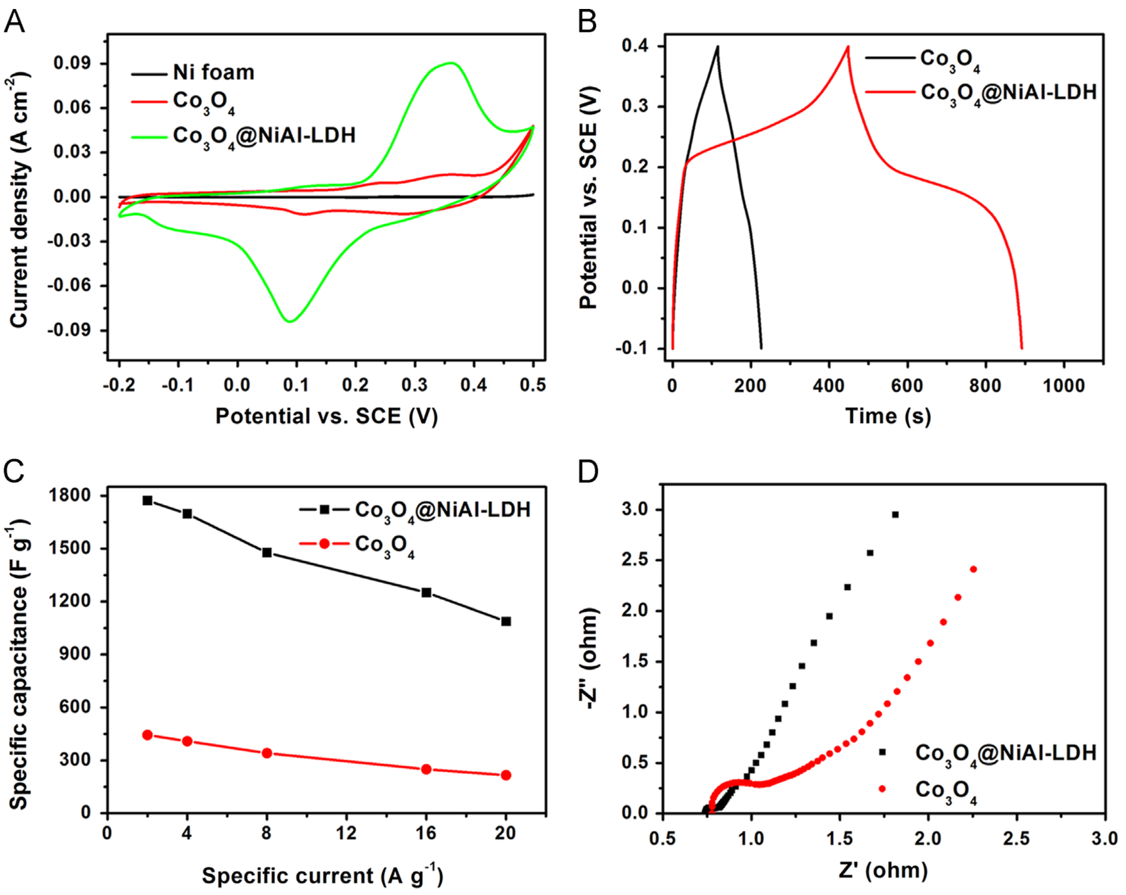

Figure 6 (A) Cyclic voltammetry (CV) curves, (B) galvanostatic (GV) charge/discharge curves, (C) current density dependence of the specific capacitance, and (D) Nyquist plots of EIS for the Co_3O_4 nanowire arrays and Co_3O_4@NiAl-LDH core/shell nanowire arrays, respectively.

originates from the hierarchical porous architecture, which enables sufficient exposure of pseudocapacitance-active components. Furthermore, the chemical binding between the Co_3O_4 core and LDH shell facilitates the charge transportation process between active components and the current collector, which contributes to the superior rate capability.

The enhanced electrochemical performance of Co_3O_4@NiAl-LDH core/shell nanowire arrays was further confirmed by the electrochemical impedance spectroscopy (EIS) measurements. Figure 6D shows the Nyquist plots of the EIS spectra for Co_3O_4@NiAl-LDH and Co_3O_4 nanowire arrays. Both curves consist of a semicircle in high frequency region and a straight line in low frequency region. The semicircle diameter reflects the charge transfer resistance, and the slope of straight line indicates the ion diffusion resistance. The Co_3O_4@NiAl-LDH core/shell nanowire arrays exhibit smaller semicircle diameter and larger slope than those of Co_3O_4, which indicates faster electron transport kinetics and ion diffusion rate for Co_3O_4@NiAl-LDH at the electrode/electrolyte interface [21,60]. For both Co_3O_4 and NiAl-LDH, the redox process involves the reversible uptaken and release of OH^- from the solution associated with electron transfer from/to the current collector [61,62]. The hierarchical porous structure of LDH shell facilitates the effective exposure of surface active sites for this Faradic redox reaction and thus benefits the interfacial charge transportation process.

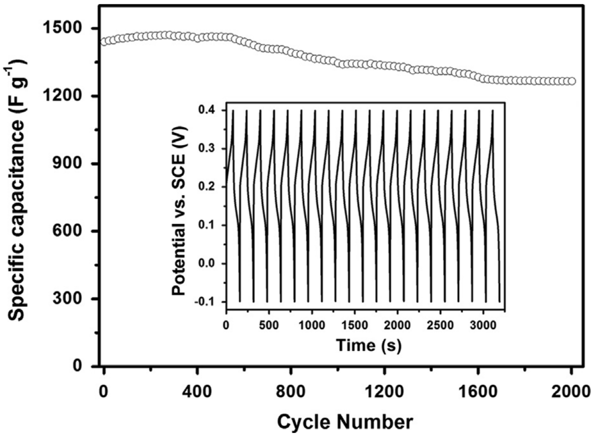

Figure 7 Cycling performance of the Co_3O_4@NiAl-LDH core/shell nanowire arrays (2000 cycles) at a large current density of $8\ \mathrm{A\,g^{-1}}$. The inset shows the charge/discharge curves of the last 20 cycles.

The cycling capability of Co_3O_4@NiAl-LDH core/shell nanowire arrays was tested for 2000 cycles at a current density of $8\ \mathrm{A\,g^{-1}}$ using galvanostatic charge/discharge measurements in the potential range from −0.1 to 0.4 V. As shown in Figure 7, the specific capacitance of Co_3O_4@NiAl-LDH maintains 87.9% after 2000 cycles. In addition, the long-term electrochemical stability can be further verified by the very stable charge/discharge curve for the last 20 cycles (inset of Figure 7, the Coulombic efficiency is ~98.8%). After long-term cycling, the ordered array structure and hierarchical morphology of Co_3O_4@NiAl-LDH core/shell nanowire arrays (Figure S8) were maintained, demonstrating its satisfactory cycling stability.

Conclusion

In conclusion, hierarchical Co_3O_4@LDH core/shell nanowire arrays have been successfully fabricated *via* a facile and cost-effective *in situ* growth method. The resulting Co_3O_4@NiAl-LDH exhibits significantly enhanced supercapacitance performance, including higher specific capacitance and superior rate capability. This can be ascribed to the hierarchical porous architecture of LDH shell and the strong core-shell chemical binding, which enables sufficient exposure of active species and benefits the charge transportation process. In addition, this synthetic approach can be extended to the preparation of Co_3O_4@MgAl-LDH and Co_3O_4@ZnAl-LDH core/shell nanowire arrays with prospective physical and chemical properties. Therefore, this work demonstrates the fabrication of hierarchical Co_3O_4@LDH core/shell nanowire arrays, which have potential applications in energy storage and conversion devices.

Acknowledgments

This work was supported by the 973 Program (Grant no. 2011CBA00504), the National Natural Science Foundation of China (NSFC), the Scientific Fund from Beijing Municipal Commission of Education (20111001002) and the Fundamental Research Funds for the Central Universities (ZD 1303). M. Wei particularly appreciates the financial aid from the China National Funds for Distinguished Young Scientists of the NSFC.

Appendix A. Supporting information

Supplementary data associated with this article can be found in the online version at http://dx.doi.org/10.1016/j.nanoen.2014.05.002.

References

[1] M. Law, L.E. Greene, J.C. Johnson, R. Saykally, P.D. Yang, Nat. Mater. 4 (2005) 455-459.
[2] W.X. Guo, C. Xu, G. Zhu, C.F. Pan, C.J. Lin, Z.L. Wang, Nano Energy 1 (2012) 176-182.
[3] Z.L. Wang, J.H. Song, Science 312 (2006) 242-246.
[4] Y. Qin, X.D. Wang, Z.L. Wang, Nature 451 (2008) 809-813.
[5] M.C. McAlpine, H. Ahmad, D. Wang, J.R. Heath, Nat. Mater. 6 (2007) 379-384.
[6] X.H. Xia, J.P. Tu, Y.Q. Zhang, Y.J. Mai, X.L. Wang, C.D. Gu, X.B. Zhao, RSC Adv. 2 (2012) 1835-1841.
[7] Y.G. Li, B. Tan, Y.Y. Wu, Nano Lett. 8 (2008) 265-270.
[8] P.H. Yang, X. Xiao, Y.Z. Li, Y. Ding, P.F. Qiang, X.H. Tan, W.J. Mai, Z.Y. Lin, W.Z. Wu, T.Q. Li, H.Y. Jin, P.Y. Liu, J. Zhou, C.P. Wong, Z.L. Wang, ACS Nano 7 (2013) 2617-2626.
[9] P.H. Yang, Y. Ding, Z.Y. Lin, Z.W. Chen, Y.Z. Li, P.F. Qiang, M. Ebrahimi, W.J. Mai, C.P. Wong, Z.L. Wang, Nano Lett. 14 (2014) 731-736.
[10] P.H. Yang, Y.Z. Li, Z.Y. Lin, Y. Dong, S. Yue, C.P. Wong, X. Cai, S.Z. Tan, W.J. Mai, J. Mater. Chem. A 2 (2014) 595-599.
[11] X.J. Feng, K. Shankar, O.K. Varghese, M. Paulose, T.J. Latempa, C.A. Grimes, Nano Lett. 8 (2008) 3781-3786.
[12] C.K. Xu, J.M. Wu, U.V. Desai, D. Gao, J. Am. Chem. Soc. 133 (2011) 8122-8125.
[13] S.H. Ko, D. Lee, H.W. Kang, K.H. Nam, J.Y. Yeo, S.J. Hong, C.P. Grigoropoulos, H.J. Sung, Nano Lett. 11 (2011) 666-671.
[14] I.S. Cho, Z.B. Chen, A.J. Forman, D.R. Kim, P.M. Rao, T.F. Jaramillo, X.L. Zheng, Nano Lett. 11 (2011) 4978-4984.
[15] C.W. Cheng, W.N. Ren, H.F. Zhang, Nano Energy 5 (2014) 132-138.
[16] Y.G. Guo, J.S. Hu, L.J. Wan, Adv. Mater. 20 (2008) 2878-2887.
[17] Y.K. Sun, S.T. Myung, B.C. Park, J. Prakash, I. Belharouak, K. Amine, Nat. Mater. 8 (2009) 320-324.
[18] Y.J. Hwang, C.H. Wu, C. Hahn, H.E. Jeong, P.D. Yang, Nano Lett. 12 (2012) 1678-1682.
[19] L. Yu, G.Q. Zhang, C.Z. Yuan, X.W.D. Lou, Chem. Commun. 49 (2013) 137-139.
[20] J.P. Liu, J. Jiang, C.W. Cheng, H.X. Li, J.X. Zhang, H. Gong, H.J. Fan, Adv. Mater. 23 (2011) 2076-2081.
[21] X.H. Xia, J.P. Tu, Y.Q. Zhang, X.L. Wang, C.D. Gu, X.B. Zhao, H.J. Fan, ACS Nano 6 (2012) 5531-5538.
[22] G.H. Zhang, T.H. Wang, X.Z. Yu, H.N. Zhang, H.G. Duan, B.G. Lu, Nano Energy 2 (2013) 586-594.
[23] J. Jiang, J.H. Zhu, Y.M. Feng, J.P. Liu, X.T. Huang, Chem. Commun. 48 (2012) 7471-7473.
[24] X.H. Xia, J.P. Tu, Y.Q. Zhang, J. Chen, X.L. Wang, C.D. Gu, C. Guan, J.S. Luo, H.J. Fan, Chem. Mater. 24 (2012) 3793-3799.
[25] W. Tian, X. Wang, C.Y. Zhi, T.Y. Zhai, D.Q. Liu, C. Zhang, D. Golberg, Y. Bando, Nano Energy 2 (2013) 754-763.
[26] B. Liu, J. Zhang, X.F. Wang, G. Chen, D. Chen, C.W. Zhou, G.Z. Shen, Nano Lett. 12 (2012) 3005-3011.
[27] J.W. Zhao, Z.Z. Lu, M.F. Shao, D.P. Yan, M. Wei, D.G. Evans, X. Duan, RSC Adv. 3 (2012) 1045-1049.
[28] R. Liu, S.B. Lee, J. Am. Chem. Soc. 130 (2008) 2942-2943.
[29] X.H. Zhao, P. Wang, B.J. Li, Chem. Commun. 46 (2010) 6768-6770.
[30] J. Chen, X.H. Xia, J.P. Tu, Q.Q. Xiong, Y.X. Yu, X.L. Wang, C.D. Gu, J. Mater. Chem. 22 (2012) 15056-15061.
[31] A. Marcu, T. Yanagida, K. Nagashima, K. Oka, H. Tanaka, T. Kawai, Appl. Phys. Lett. 92 (2008) 173119.
[32] Z.P. Xu, P.S. Braterman, J. Phys. Chem. C 111 (2007) 4021-4026.
[33] Z.P. Xu, P.S. Braterman, Appl. Clay Sci. 48 (2010) 235-242.
[34] B. Sels, D.D. Vos, M. Buntinx, F. Pierard, K.D. Mesmaeker, P. Jacobs, Nature 400 (1999) 855-857.
[35] G. Busca, U. Costantino, T. Montanari, G. Ramis, C. Resini, M. Sisani, Int. J. Hydrog. Energy 35 (2010) 5356-5366.
[36] J.L. Gunjakar, T.W. Kim, H.N. Kim, I.Y. Kim, S.J. Hwang, J. Am. Chem. Soc. 133 (2011) 14998-15007.
[37] D.P. Yan, J. Lu, M. Wei, S.H. Qin, L. Chen, S.T. Zhang, D.G. Evans, X. Duan, Adv. Funct. Mater. 21 (2011) 2497-2505.
[38] M.F. Shao, M. Wei, D.G. Evans, X. Duan, Chem. Commun. 47 (2011) 3171-3173.
[39] Z. Gu, A.C. Thomas, Z.P. Xu, J.H. Campbell, G.Q. Lu, Chem. Mater. 20 (2008) 3715-3722.
[40] Q. Wang, D. O'Hare, Chem. Rev. 112 (2012) 4124-4155.
[41] A.B. Béléké, M. Mizuhata, J. Power Sources 195 (2010) 7669-7676.
[42] Y.G. Wang, L. Cheng, Y.Y. Xia, J. Power Sources 153 (2006) 191-196.

[43] J.B. Han, Y.B. Dou, J.W. Zhao, M. Wei, D.G. Evans, X. Duan, Small 9 (2013) 98-106.
[44] Z. Gao, J. Wang, Z. Li, W. Yang, B. Wang, M. Hou, Y. He, Q. Liu, T. Mann, P. Yang, Chem. Mater. 23 (2011) 3509-3516.
[45] L.J. Zhang, J. Wang, J.J. Zhu, X.G. Zhang, K.S. Hui, K.N. Hui, J. Mater. Chem. A 1 (2013) 9046-9053.
[46] J. Xu, S.L. Gai, F. He, N. Niu, P. Gao, Y.J. Chen, P.P. Yang, J. Mater. Chem. A 2 (2014) 1022-1031.
[47] M.F. Shao, F.Y. Ning, Y.F. Zhao, J.W. Zhao, M. Wei, D.G. Evans, X. Duan, Chem. Mater. 24 (2012) 1192-1197.
[48] Y.H. Gu, Z.Y. Lu, Z. Chang, J.F. Liu, X.D. Lei, Y.P. Li, X.M. Sun, J. Mater. Chem. A 1 (2013) 10655-10661.
[49] X.H. Xia, J.P. Tu, X.L. Wang, C.D. Gu, X.B. Zhao, Chem. Commun. 47 (2011) 5786-5788.
[50] Q. Yang, Z.Y. Lu, Z. Chang, W. Zhu, J.Q. Sun, J.F. Liu, X.M. Sun, X. Duan, RSC Adv. 2 (2012) 1663-1668.
[51] J. Jiang, J.P. Liu, X.T. Huang, Y.Y. Li, R.M. Ding, X.X. Ji, Y.Y. Hu, Q.B. Chi, Z.H. Zhu, Cryst. Growth Des. 10 (2010) 70-75.
[52] Y.F. Zhao, S. He, M. Wei, D.G. Evans, X. Duan, Chem. Commun. 46 (2010) 3031-3033.
[53] K.B. Kim, J. Das, F. Baier, J. Eckert, Appl. Phys. Lett. 86 (2005) 201909.
[54] K. Cheng, F. Yang, G.L. Wang, J.L. Yin, D.X. Cao, J. Mater. Chem. A 1 (2013) 1669-1676.
[55] J.K. Chang, C.M. Wu, I.W. Sun, J. Mater. Chem. 20 (2010) 3729-3735.
[56] Q.W. Huang, S.Q. Tian, D.W. Zeng, X.X. Wang, W.L. Song, Y.Y. Li, W. Xiao, C.S. Xie, ACS Catal. 3 (2013) 1477-1485.
[57] M. Wei, X.Y. Xu, X.R. Wang, F. Li, H. Zhang, Y.L. Lu, M. Pu, D. G. Evans, X. Duan, Eur. J. Inorg. Chem. 2006 (2006) 2831-2838.
[58] X.H. Huang, G.H. Li, B.Q. Cao, M. Wang, C.Y. Hao, J. Phys. Chem. C 113 (2009) 4381-4385.
[59] G.W. Yang, C.L. Xu, H.L. Li, Chem. Commun. 44 (2008) 6537-6539.
[60] J.F. Zang, S.J. Bao, C.M. Li, H.J. Bian, X.Q. Cui, Q.L. Bao, C.Q. Sun, J. Guo, K.R. Lian, J. Phys. Chem. C 112 (2008) 14843-14847.
[61] R. Kötz, M. Carlen, Electrochim. Acta 45 (2000) 2483-2498.
[62] J. Liu, C. Cheng, W. Zhou, H. Li, H.J. Fan, Chem. Commun. 47 (2011) 3436-3438.

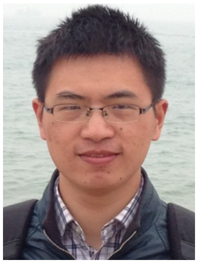

Fanyu Ning received his Bachelor's degree from Beijing University of Chemical Technology (BUCT) in Applied Chemistry in 2011. He is now a Ph.D. candidate under the supervision of Prof. Min Wei in the BUCT. His research interests mainly focus on the design and fabrication of layered double hydroxides nanostructures for energy storage and conversion.

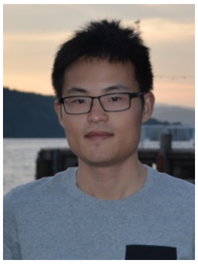

Mingfei Shao is currently pursuing his Ph.D. degree under the supervision of Prof. Xue Duan in Beijing University of Chemical Technology, China. His current research interests are mainly focused on the controlled synthesis of layered functional materials and their applications in electrochemistry, catalysis as well as separation.

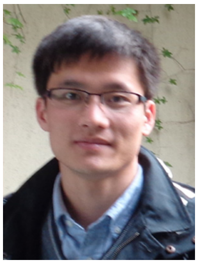

Chenglong Zhang received his Bachelor's degree in 2012 from China University of Mining and Technology (CUMT), China. He is currently a postgraduate in Beijing University of Chemical Technology (BUCT) under the supervision of Prof. Min Wei. His research interests mainly focus on design of functional nanomaterials and fabrication of photoelectrode for photoelectrochemical water splitting.

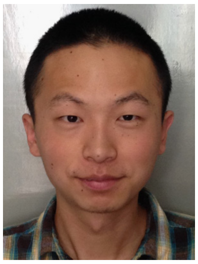

Simin Xu received his Bachelor's degree from Beijing University of Chemical Technology (BUCT) in Applied Chemistry in 2011. He is now a Ph.D. candidate under the supervision of Prof. Xue Duan in the BUCT. His research interests mainly focus on the experimental and computational investigation of the physical and chemical properties of layered double hydroxides.

Min Wei obtained her B.Eng. degree in 1995 and M.Eng. degree in 1998 from Beijing University of Chemical Technology (BUCT). She subsequently received her Ph.D. from Peking University in 2001, after which she joined to the staff of BUCT. She was promoted to full Professor in 2005. She has been a visiting scholar in the Georgia Institute of Technology (in 2008). Her research interests focus on inorganic-organic composite functional materials as well as new catalysts.

Xue Duan was elected as an Academician of the Chinese Academy of Sciences in 2007. He was awarded his B.S. degree from Jilin University and M.S. and Ph.D. degrees from Beijing University of Chemical Technology (BUCT). He was subsequently appointed to the staff of BUCT and established the Applied Chemistry Research Institute in 1990. He was promoted to full Professor in 1993 and to Ph.D. supervisor status in 1995. He is currently the Director of the Institute of Applied Chemistry and Executive Vice-Chair of the Academic Committee of the State Key Laboratory of Chemical Resource Engineering.